Antitumor Agents

How to cite:
International Edition: doi.org/10.1002/anie.202200237
German Edition: doi.org/10.1002/ange.202200237

Ferrocene-Containing Nucleic Acid-Based Energy-Storage Nanoagent for Continuously Photo-Induced Oxidative Stress Amplification

Cailing Ji[+], Hao Li[+], Lei Zhang[+], Ping Wang, Yawei Lv, Zhijun Sun, Jie Tan,* Quan Yuan,* and Weihong Tan*

Abstract: *Regulation of cellular oxidative stress plays a critical role in revealing the molecular mechanisms of cellular activities and thus is a potential strategy for tumor treatment. Optical methods have been employed for intelligent regulation of oxidative stress in tumor regions. However, long-time continuous irradiation inevitably causes damage to normal tissues. Herein, a ferrocene-containing nucleic acid-based energy-storage nanoagent was designed to achieve the continuous photo-regulation of cellular oxidative stress in the dark. Specifically, the photoenergy stored in the agent could convert effectively and accelerate Fenton-like reaction continuously, augmenting cellular oxidative stress. This nanoagent could also silence oxidative damage repair genes to further amplify oxidative stress. This strategy not only provides oxidative stress regulation for studying the molecular mechanisms of biological activities, but also offers a promising step toward tumor microenvironment modulation.*

Introduction

Cellular oxidative stress is an imbalanced redox status caused by augmenting reactive oxygen species (ROS) production or suppressing antioxidant mechanisms.[1] Excessive oxidative stress may trigger apoptosis or necrosis via the irreversible oxidative damage to biomacromolecules in living cells.[2] Oxidative stress in tumor cells is found typically higher than normal cells.[3] As the expression of endogenous antioxidants upregulated, tumor cells would be in an equilibrium state and more sensitive to adapt to high oxidative stress that exceeds the cellular tolerability threshold.[1c,4] Therefore, the regulation of oxidative stress in tumor cells is expected to disrupt the balance status, achieving excellent antitumor therapeutic efficacy.

By photoenergy conversion, optical methods can realize intelligent regulation of oxidative stress and have grown into an indispensable tool in oxidative stress modulation.[5] During light irradiation, the photosensitizer can absorb and convert photoenergy into chemical energy via photon–electron interactions, inducing oxidation reaction upon real-time light excitation.[5a,6] However, in the process of photo-driven oxidative stress regulation, most of the photoenergy will be absorbed by biological samples and be converted into local heat energy.[5b,7] The prolonged strong light irradiation may thus lead to possible local overheating and further cause severe damage to normal cells and tissues.[8] If photoenergy can be stored in the photosensitizer to achieve constant regulation of oxidative stress after illumination, side effects such as tissue damage caused by prolonged light irradiation can be effectively avoided.

Persistent luminescence nanomaterials can store excitation energy under light irradiation, enabling persistent luminescence after excitation ceases.[9] Thus, the persistent luminescence nanomaterials act as an optical battery to trap photoenergy in defects and slowly release the stored energy by chemical/physical activation, eliminating the need for constant light irradiation.[10] Inspired by this, we report the use of persistent luminescence nanomaterials to fabricate an energy-storage nanoagent with ferrocene-containing nucleic acids for continuously photo-activated oxidative stress amplification. Persistent luminescence nanomaterials in this nanoagent can store photoenergy, making prolonged light irradiation unnecessary. By photoenergy conversion, ferrocene-containing nucleic acids in the energy-storage nanoagent can initiate a Fenton-like reaction to exacerbate the oxidant environment. In vitro and in vivo studies indicate that, after cessation of excitation, the nanoagent could sustainedly induce the production of oxygen species in the dark, aggravating the oxidative stress in the tumor microenvironment constantly. Additionally, this nanoagent can integrate siRNA to silence oxidative damage repair genes in

[*] C. Ji,[+] L. Zhang,[+] Y. Lv, J. Tan, Prof. Q. Yuan, Prof. W. Tan
Molecular Science and Biomedicine Laboratory,
Institute of Chemical Biology and Nanomedicine,
State Key Laboratory of Chemo/Biosensing and Chemometrics,
College of Chemistry and Chemical Engineering,
School of Physics and Electronics,
Hunan University, Changsha 410082 (China)
E-mail: tanjie0416@hnu.edu.cn
yuanquan@whu.edu.cn

H. Li,[+] Prof. Z. Sun, Prof. Q. Yuan
The State Key Laboratory Breeding Base of Basic Science of Stomatology (Hubei-MOST) and Key Laboratory of Oral Biomedicine Ministry of Education, School and Hospital of Stomatology,
College of Chemistry and Molecular Sciences,
Wuhan University, Wuhan 430072 (China)
E-mail: sunzj@whu.edu.cn

Prof. P. Wang
Wuhan National Laboratory for Optoelectronics,
School of Engineering Sciences,
Huazhong University of Science and Technology,
Wuhan 430074 (China)

[+] These authors contributed equally to this work.

tumor cells, inhibiting the cellular antioxidant defense system and further potentiating oxidative stress.[11] This energy-storage nanoagent enables oxidative stress regulation, providing a promising strategy for studying the molecular mechanisms of biological activities and for further application in potential areas such as tumor microenvironment modulation and metabolic pathway regulation.

Results and Discussion

A siRNA-aptamer-ferrocene modified persistent luminescence nanoparticle (siRNA-ApFe-PLNP) was designed as an energy-storage nanoagent to achieve continuous amplification of oxidative stress after photo-activation, eliminating the need for constant light irradiation and further avoiding photo-induced tissue damage.[12] By initiating the Fenton-like reaction, ferrocene is usually applied to amplify oxidative stress.[13] As shown in Scheme 1, under light irradiation, PLNP not only serve as an energy storage core to absorb and store photoenergy, but also can generate hydroxyl radicals ($^{\bullet}OH$) via photocatalysis.[8b,12] Upon removal of the excitation source, the energy stored in PLNP will transfer and accelerate Fe^{III}/Fe^{II} conversion. Then Fenton-like reaction can be activated sustainably to realize continuous oxidative stress amplification. On the other hand, tumor cells have diversified oxidative damage repair genes that encode repair proteins such as MTH1 protein to prevent excessive oxidative stress.[11c,14] On this basis, siRNA was introduced to suppress the expression of MTH1 protein by silencing oxidative repair-related genes in tumor cells. The resulting inhibition of oxidative damage repair will further aggravate oxidative stress.

The preparation process of siRNA-ApFe-PLNPs was displayed in Figure 1a. PLNPs were prepared according to the method described in our previous work (Figure S1).[9c,15] PLNPs and ferrocene-containing nucleic acids were self-assembled to form siRNA-ApFe-PLNPs by a phase transfer method (Figure S2).[16] Nucleic acid polymers used here bore three distinct domains. The yellow domain is hydrophobic ferrocene nucleotides (Fe bases) that self-assemble with the hydrophobic PLNP core (Figures S3–S5). Rest two domains are two hydrophilic DNA chains, including a tail (green) and an A549 cell-targeting aptamer (purple) to enhance targeting and internalization of ApFe-PLNPs (Figure S6).[17] Owing to the tail region, ApFe-PLNPs can further integrate gene therapy agents via complementary base pairing.[18] To obtain siRNA-ApFe-PLNPs, the siRNA was integrated into the ApFe-PLNP system to repress MTH1 expression. Transmission electron microscopy (TEM) images and corresponding size distributions of PLNPs, ApFe-PLNPs and siRNA-ApFe-PLNPs were obtained with a slightly growing diameter (Figures 1b–d and S7). Elemental mapping images confirmed the successful combination of Fe bases and PLNPs (Figure S8). Moreover, dynamic light scattering (DLS) analysis results further indicated the uniform size distribution of PLNPs, ApFe-PLNPs, and siRNA-ApFe-PLNPs with a diameter of ≈30 nm, ≈40 nm, and ≈50 nm, respectively (Figures 1e–g). These observations revealed that ApFe-PLNPs and siRNA-ApFe-PLNPs displayed excellent dispersibility and uniform particle size. Together, these results proved the successful preparation of siRNA-ApFe-PLNPs. The stability of siRNA-ApFe-PLNPs was further characterized by DLS under different biological mimicking conditions within 14 days. The size of siRNA-ApFe-PLNPs remained ≈50 nm in these environments, implying the good stability of siRNA-ApFe-PLNPs in biological conditions (Figures S9–S11).

The colorimetric assay was employed to monitor whether siRNA-ApFe-PLNPs perform the continuous oxidation capability after photo-activation in vitro. 3,3′,5,5′-tetramethylbenzidine (TMB) was utilized to explore the oxygen specie production. Hydroxyl radicals generated by siRNA-ApFe-PLNPs can oxidize TMB from colorless to

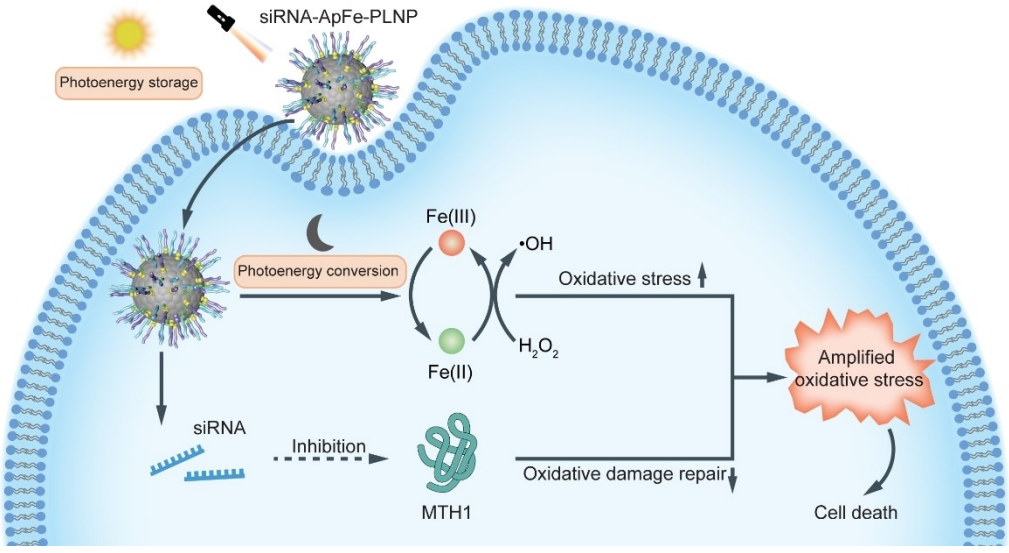

Scheme 1. Schematic illustration of photo-activated siRNA-ApFe-PLNPs to continuously amplify cellular oxidative stress in the dark.

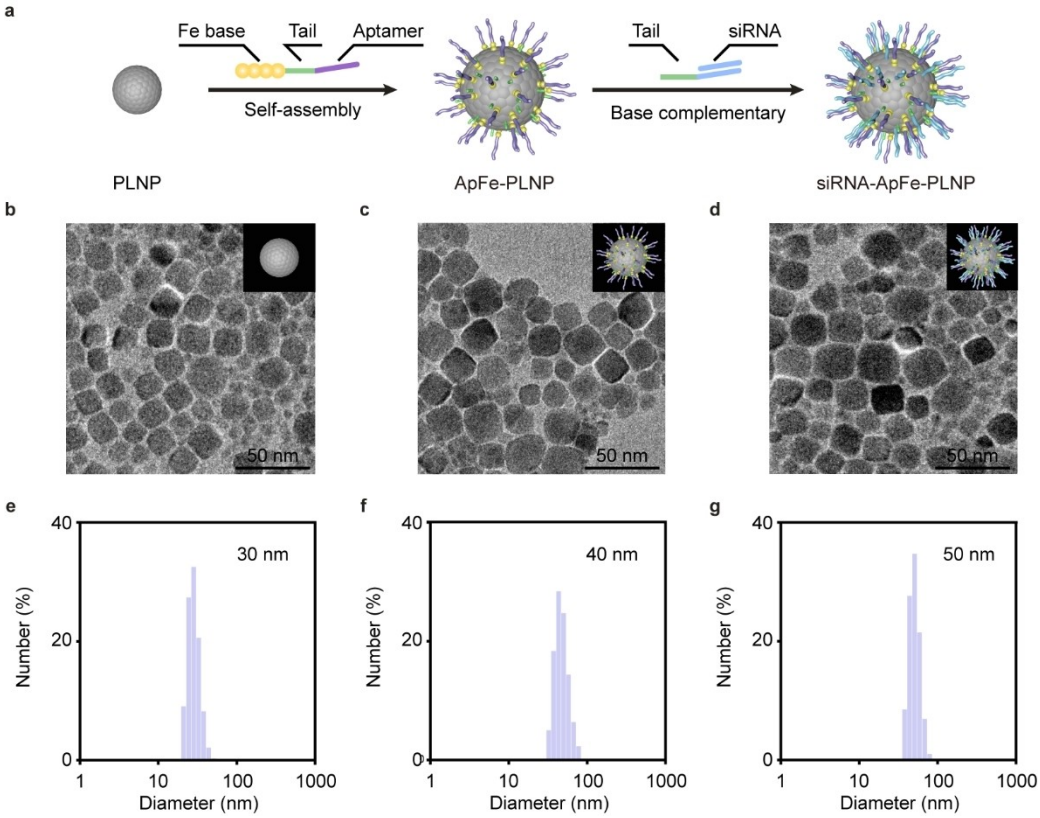

Figure 1. Synthesis and characterization of siRNA-ApFe-PLNPs. a) Schematic of the synthesis process of siRNA-ApFe-PLNPs. TEM images of PLNPs (b), ApFe-PLNPs (c), and siRNA-ApFe-PLNPs (d), respectively. Size determination of PLNPs (e), ApFe-PLNPs (f), and siRNA-ApFe-PLNPs (g) via DLS, respectively. Scale bar, 50 nm.

chromogen TMB cation-free radicals with a typical absorption peak at 652 nm.[19] After the stoppage of light, the spectral signal of PLNPs displayed no significant change, whereas the signal of siRNA-ApFe-PLNPs kept rising (Figure S12). This phenomenon elucidated that, owing to the modification of Fe bases, the photoenergy stored in siRNA-ApFe-PLNPs could continuously induce the occurrence of oxidation reaction after photo-excitation. Density functional theory calculations further illustrated that the oxygen vacancies in PLNPs might induce the deep traps, making siRNA-ApFe-PLNPs have superb capacities in energy collection, storage, and conversion (Figure S13). To investigate the impact of the ferrocene moieties, siRNA-ApFe-PLNPs containing different amounts of Fe bases were prepared and their continuous oxidative ability was evaluated by colorimetric assay (Figures S14–S19, and Table S1). After light excitation, the time-course absorbance of PLNPs and siRNA-ApFe-PLNPs with 3, 6, or 9 Fe bases was obtained (Figure S20). These curves presented that the absorbance of PLNPs and siRNA-ApFe-PLNPs with 3, 6, or 9 Fe bases all showed a rising trend, and the most significant increase was found in siRNA-ApFe-PLNPs with 9 Fe bases. Then the corresponding maximum relative velocity was calculated according to the time-course absorption curve.[20] The velocity was found accelerating with the addition of Fe bases, indicating that siRNA-ApFe-PLNPs enhanced the production of hydroxyl radicals due to the increasing Fe bases (Figure 2a). The inserted photograph in Figure 2a intuitively presented the chromogenic changes and the siRNA-ApFe-PLNPs with 9 Fe bases turned blue clearly, agreeing well with the results of time-course absorbance assay (Figures S21, S22). These observations revealed that the continuous oxidation capacity of siRNA-ApFe-PLNPs enhanced with the increase of Fe bases, since the increasing Fe bases could promote the conversion efficiency of photoenergy into chemical energy, thereby accelerating the oxidation reaction. The hydroxyl radical generation rate of siRNA-ApFe-PLNPs with 9 Fe bases was further investigated using typical Michaelis–Menten steady-state kinetics (Figure S23). The K_M and V_{max} values for siRNA-ApFe-PLNPs were calculated to be 1.3 mM and $2.7\times10^{-9}\,M\,s^{-1}$, respectively. Subsequently, the continuous oxidation capacity caused by photoenergy storage and conversion of siRNA-ApFe-PLNPs after excitation was further evaluated by electron paramagnetic resonance (EPR) spectroscopy. 5,5-dimethyl-1-pyrroline-N-oxide (DMPO) was applied to obtain radical-DMPO adducts.[21] The EPR signals of PLNPs and siRNA-ApFe-PLNPs with 3, 6, or 9 Fe bases were obtained before or after photo-activation. Under dark conditions, no signal was detected in PLNPs with or without Fe base-modification, demonstrating that these materials displayed the inability for photoenergy transformation to amplify oxidative stress without photo-activation (Figure S24). After photo-activation, bare PLNPs showed weak

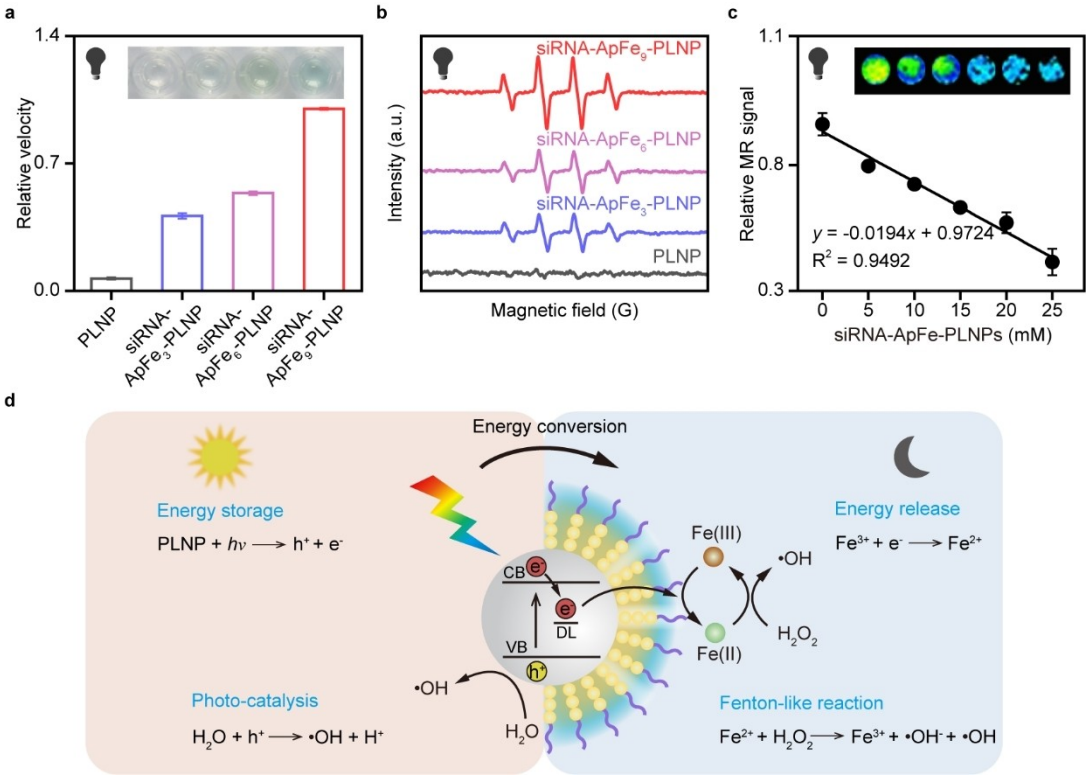

Figure 2. siRNA-ApFe-PLNPs continuously undergo oxidative reaction after photo-activation. a) Photographs (top) and maximum relative velocity (bottom) of hydroxyl radical generated by PLNPs (black column) and siRNA-ApFe-PLNPs containing 3 (blue column), 6 (pink column), or 9 (red column) bases after light irradiation. Data are presented as the mean ± s.d.; $n = 3$. b) EPR spectra of DMPO/hydroxyl radical adducts for PLNPs (black line) and siRNA-ApFe-PLNPs containing 3 (blue line), 6 (pink line), or 9 (red line) Fe bases after light irradiation. c) T2-weighted images (top) and corresponding quantitative data analysis (bottom) of siRNA-ApFe-PLNPs at different concentrations after light irradiation. Data are presented as the mean ± s.d.; $n = 3$. d) Detailed mechanisms of continuously initiated oxidative reaction by siRNA-ApFe-PLNPs. CB, conduction band; VB, valence band; DL, defect level.

signals, while typical 1:2:2:1 four-line hydroxyl radical signals appeared pronouncedly in siRNA-ApFe-PLNPs (Figure 2b). These phenomena manifested that siRNA-ApFe-PLNPs could continue to enhance the hydroxyl radical production in the dark after photo-excitation. It was worth noting that with the increase of Fe bases, the elevated hydroxyl radical signals commenced remarkably, and the similar results were also observed under light conditions (Figures S25, S26). Altogether, siRNA-ApFe-PLNPs exhibited the ability to store and convert photoenergy into chemical energy, achieving the continuous oxidative stress amplification after photo-activation. Besides, the conversion efficiency was positively correlated with the number of Fe bases. Furthermore, thermoluminescence and the persistent luminescence decay analyses were performed and showed that the energy stored in siRNA-ApFe-PLNPs with 9 Fe bases could be kept in the dark for more than 60 min (Figures S27–S36). As a result, considering their excellent energy conversion ability without prolonged excitation, siRNA-ApFe-PLNPs containing 9 Fe bases were selected for subsequent research.

During the Fenton-like reaction activated by photo-energy conversion, Fe^{II} in ferrocene moieties can be oxidized to Fe^{III}, a negative contrast agent for magnetic resonance imaging (MRI).[22] MRI was thus used to illustrate the Fenton-like reaction progress induced by the photo-energy conversion of photo-activated siRNA-ApFe-PLNPs.[23] After illumination, T2-weighted magnetic resonance (MR) images were acquired and revealed a notable loss in signal with increasing siRNA-ApFe-PLNPs concentration, indicating the effective Fe^{III} production (Figure 2c, insert). The quantitative analysis in Figure 2c illustrated a linear correlation between the MR signal intensity and the siRNA-ApFe-PLNPs concentrations, confirming the dose-dependent reduction of MR signal. MRI observations proved that siRNA-ApFe-PLNPs could generate Fe^{III} sustainably via Fenton-like reaction after the cessation of excitation, in consistent with the results of EPR spectroscopy. Collectively, siRNA-ApFe-PLNPs could constantly initiate Fenton-like reaction sustainably via photoenergy conversion after excitation ceased, exhibiting a continuous oxidation ability. Therefore, it might be possible that due to the photoenergy storage and conversion, siRNA-ApFe-PLNPs could achieve continuous photo-driven regulation of oxidative stress under dark conditions. To explore energy transfer-induced Fe^{II}/Fe^{III} conversion, TMB-colorimetric assay and MRI were also performed on ferrocene, PLNPs, PLNPs + ferrocene and siRNA-ApFe-PLNPs, respectively.

These results manifested that owing to the energy transfer between Fe-bases and PLNPs, siRNA-ApFe-PLNPs accelerated the Fe^{II}/Fe^{III} conversion after photo-excitation and continuously underwent Fenton-like reactions to produce hydroxyl radicals (Figures S37–S41). Based on the above-mentioned results, a possible mechanism for oxidative stress amplification by siRNA-ApFe-PLNPs is proposed in Figure 2d. Under light irradiation, siRNA-ApFe-PLNPs are activated to generate charge carriers and store partial of them. In addition, some of photogenerated charge carriers can realize the photocatalytic reaction to produce hydroxyl radicals [Eqs. (1) and (2)].[9a,12,24]

$$\text{PLNPs} + h\nu \rightarrow h^+ + e^- \quad (1)$$

$$H_2O + h^+ \rightarrow {}^{\bullet}OH + H^+ \quad (2)$$

$$Fe^{2+} + H_2O_2 \rightarrow Fe^{3+} + {}^{\bullet}OH^- + {}^{\bullet}OH \quad (3)$$

$$Fe^{3+} + H_2O_2 \rightarrow Fe^{2+} + H^+ + {}^{\bullet}OOH \quad (4)$$

Ferrocene moieties can undergo a Fenton-like reaction under oxidative conditions [Eqs. (3) and (4)].[13,24,25] After excitation ceases, the charge carriers stored in PLNPs will transfer to ferrocene and accelerate the Fe^{II}/Fe^{III} conversion, thus enabling Fenton-like reaction persistently in the dark. Owing to the ability for photoenergy storage and conversion without sustained excitation, siRNA-ApFe-PLNPs performed continuous oxidation ability after photo-activation, holding the potential to be applied as an oxidative stress amplifier.

Compared to normal cells, tumor cells characteristically display a significant high oxidative stress[3a,b,4b] In response to the high oxidative stress, tumor cells have diversified oxidative damage repair genes to encode a series of enzymes that can repair oxidative damage, resulting in the resistance to oxidative therapeutic drugs.[11c,14] For instance, MTH1 protein can sanitize oxidized nucleotide pools, significantly repairing oxidative damage in tumor cells.[14a,19b] It is reported that suppressing the repair of oxidative damage can notably enhance oxidative stress in tumor cells.[11a,23d] To realize the effective regulation of oxidative stress in tumor cells, the oxidative stress amplifier requires to overcome the oxidative damage repair. Here, the siRNA that inhibits MTH1 expression was integrated in siRNA-ApFe-PLNPs to impede the MTH1-mediated oxidative damage repairing process and to regulate oxidative stress in tumor cells. With base complementary pairing, MTH1 siRNA was integrated in the siRNA-ApFe-PLNPs (Figure 3a). To identify the inhibitory effect of siRNA-ApFe-PLNPs on MTH1 expression, western blot analysis was employed and A549 cell line was selected as the tumor cell model. Compared with the ApFe-PLNPs treated cells, MTH1 expression declined apparently in cells incubated with siRNA-ApFe-PLNPs, validating the effectiveness of siRNA-ApFe-PLNPs for suppressing MTH1 expression (Figures 3b and S42, S43). Since the amplified oxidative stress will initiate apoptotic cell death, Annexin V-PI was exploited to evaluate the oxidative stress regulation ability of PLNPs, ApFe-PLNPs and siRNA-ApFe-PLNPs via photoenergy storage and conversion in A549 cells (Figure 3c). The non-photo-activated group presented about 90 % of cell viability whereas the photo-activated group caused an obvious decrease in cell viability, implying a heightened oxidative stress regulation ability of these materials due to the energy storage and conversion after photo-excitation. Statistically, there were more dead cells in the photo-activated siRNA-ApFe-PLNPs group than that in other groups. Similar observations were obtained by the cell counting kit 8 (CCK-8) analysis (Figure 3d). These results confirmed that siRNA-ApFe-PLNPs performed the most prominent ability to store and convert photoenergy with the assistance of photo-excitation, realizing the continuous oxidative stress regulation in tumor cells.

The capacity of photoenergy stored siRNA-ApFe-PLNPs to amplify oxidative stress in tumor cells was investigated using a fluorescent ROS probe. The fluorescent probe 2,7-dichlorofluorescin diacetate (DCFH-DA) can emit green fluorescence when oxidized by ROS.[26] Based on this, DCFH-DA was utilized to evaluate the oxidative stress regulation of A549 cells incubated with PBS, ApFe-PLNPs, and siRNA-ApFe-PLNPs, respectively (Figures 3e and S44). After illumination, vivid green fluorescence was observed in cells treated with ApFe-PLNPs or siRNA-ApFe-PLNPs, proving their efficient photoenergy storage and transformation performance. Statistically, using flow cytometry, the fluorescence signal in siRNA-ApFe-PLNPs-treated cells was significantly higher than that of ApFe-PLNPs-treated cells (Figures S45, S46). The quantified data measured by confocal microscopy and flow cytometry were well matched. These observations indicated the enhanced cellar oxidative stress in siRNA-ApFe-PLNPs treated group, possibly owing to the inhibition of oxidative damage repair protein MTH1 expression. The above results revealed that, in addition to effective photoenergy conversion, energy-storage siRNA-ApFe-PLNPs could further amplify the oxidative stress in tumor cells by inhibiting oxidative damage genes. Further, PLNPs, ApFe-PLNPs, or siRNA-ApFe-PLNPs were injected intravenously into A549 tumor-bearing mice respectively to investigate their regulation capacity to oxidative stress in tumor tissues by MRI.[27] After illumination, T2-weighted contrast effect of different materials was analyzed to verify the Fenton-like reaction in vivo. Compared with the other groups, the siRNA-ApFe-PLNPs injected group exhibited a remarkable reduction of signal intensity in tumor regions (Figure 3f). The corresponding relative MR signal intensity was calculated to decrease to 30 % in siRNA-ApFe-PLNPs group (Figure S47). These negative MRI signals suggested the effective generation of Fe^{III} in siRNA-ApFe-PLNPs group via Fenton-like reaction in vivo. Collectively, all these phenomena illustrated that the photoenergy stored siRNA-ApFe-PLNP system could continuously regulate oxidative stress via photoenergy conversion in tumor cells and tumor tissues.

Encouraged by the continuous regulation of oxidative stress via photoenergy conversion in vitro, the corresponding in vivo experiments were carried out to investigate whether photoenergy stored siRNA-ApFe-PLNP as an

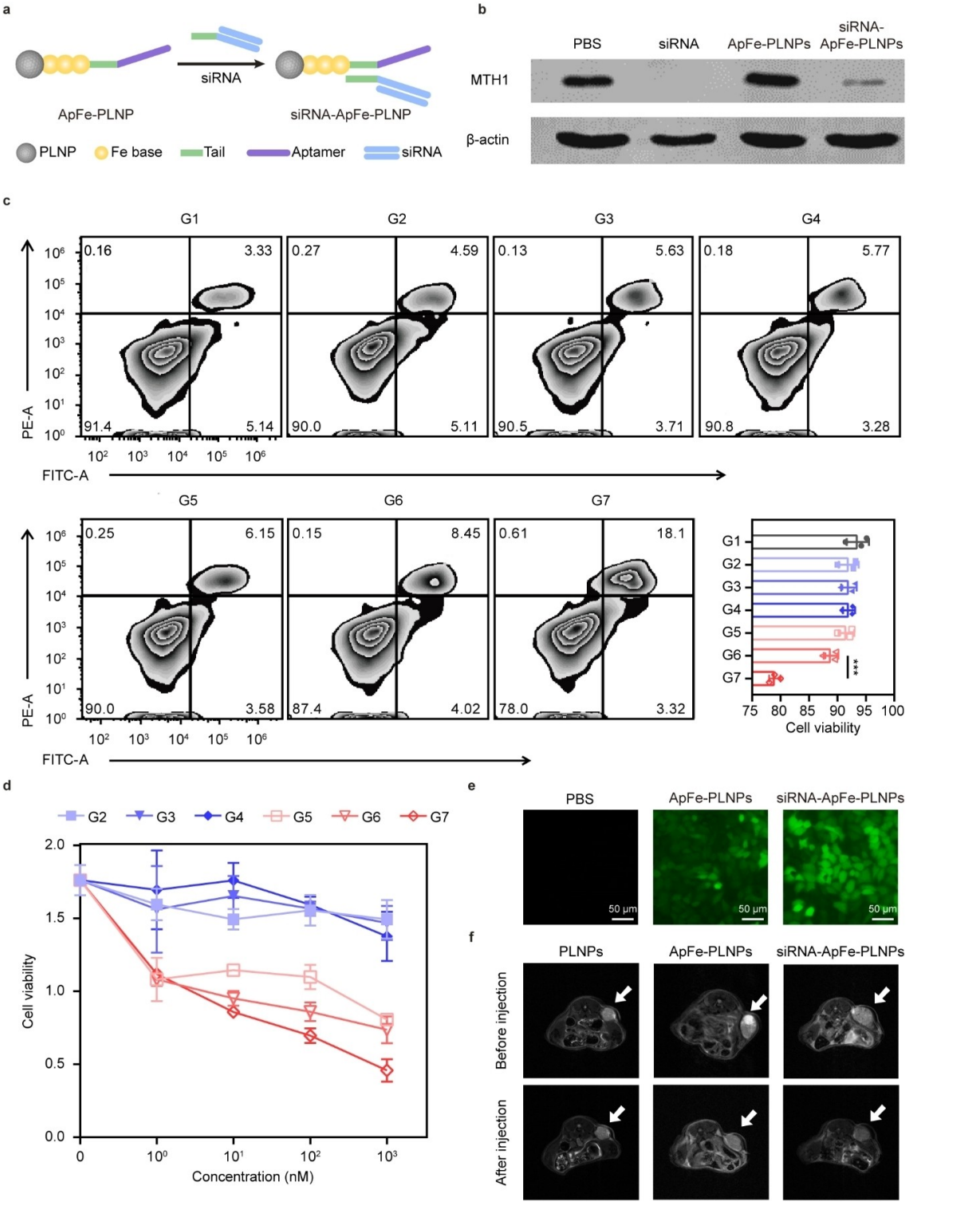

Figure 3. Photo-activated siRNA-ApFe-PLNPs amplify oxidative stress continuously in tumor cells. a) Schematic binding process of siRNA integration into siRNA-ApFe-PLNP. b) Western blot analysis of MTH1 expression in A549 cells treated with phosphate buffer saline (PBS), siRNA, ApFe-PLNPs, and siRNA-ApFe-PLNPs, respectively. c) Cell apoptosis assay for A549 cells treated with different conditions. Data are shown as the mean ± s.d.; $n = 3$; $^{***}P < 0.001$, analyzed by two-sided Student's t-test. d) Cell viability of A549 cells after different treatments by CCK8 assay. G1, PBS; G2, PLNPs; G3, ApFe-PLNPs; G4, siRNA-ApFe-PLNPs; G5, PLNPs + light; G6, ApFe-PLNPs + light; G7, siRNA-ApFe-PLNPs + light. Data are presented as the mean ± s.d.; $n = 3$. e) Intracellular ROS detection in A549 cells incubated with PBS, ApFe-PLNPs, or siRNA-ApFe-PLNPs after light irradiation using the fluorescent probe DCFH-DA. Scale bar, 50 μm. f) MRI images of A549 tumor-bearing mice before and after injection of PLNPs, ApFe-PLNPs, and siRNA-ApFe-PLNPs, respectively.

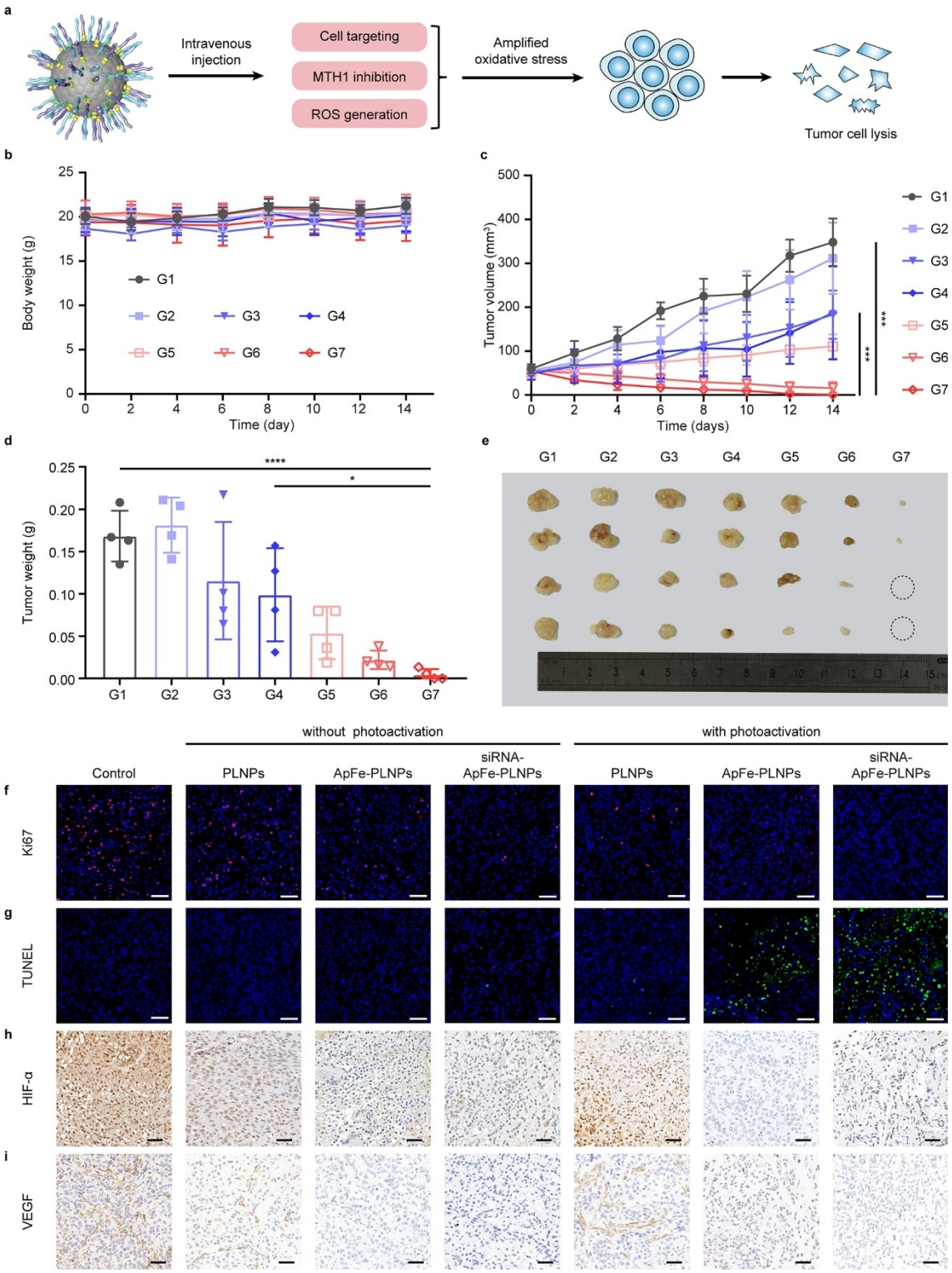

Figure 4. Photo-activated siRNA-ApFe-PLNPs amplify oxidative stress continuously and enhance tumor suppression effect. a) Schematic antitumor mechanism of siRNA-ApFe-PLNPs. Body weights (b) and tumor growth curves (c) of A549 bearing nude mice after various treatments. All the above data were collected and measured every 2 days. Each bar represents the mean ± s.d.; $n = 4$; ***$P < 0.001$, analyzed by two-sided Student's t-test. Tumor weights (d) and photographs (e) of the dissected tumors at the 14th day after different treatments. Data are presented as the mean ± s.d.; $n = 4$. *$P < 0.05$, ***$P < 0.001$, analyzed by two-sided Student's t-test. G1, PBS; G2, PLNPs; G3, ApFe-PLNPs; G4, siRNA-ApFe-PLNPs; G5, PLNPs + light; G6, ApFe-PLNPs + light; G7, siRNA-ApFe-PLNPs + light. f) The cellular proliferation in the tumor tissues by immunofluorescence staining of Ki67. g) The apoptosis in the tumor tissues by immunofluorescence staining of TUNEL. The hypoxia in the tumor tissues was analyzed by immunohistochemical staining of HIF-α (h) and VEGF (i). Scale bar, 50 μm.

oxidative stress amplifier can work for tumor therapy. The oxidative stress amplification mechanism of siRNA-ApFe-PLNPs in vivo was schematically shown in Figure 4a. Tumor-site-specific amplification of oxidative stress was reported to decrease the proliferation and to increase the apoptosis of tumor cells, achieving the efficient tumor suppression.[28] The biosafety of the siRNA-ApFe-PLNPs was evaluated by measuring their tissue and blood compatibilities on female athymic BALB/c mice (Figures S48–S51). As a result, the siRNA-ApFe-PLNPs exhibited satisfiable biosafety in the mice model, laying a good foundation for further in vivo application. The biodistribution of the nanoagents was also evaluated, elucidating that the nanoparticles displayed a good tumor accumulation efficiency (Figures S52–S56). The A549 tumor bearing nude mice were randomly divided into seven groups and received different treatments: PBS, PLNPs, ApFe-PLNPs, siRNA-ApFe-PLNPs, PLNPs + light, ApFe-PLNPs + light, and siRNA-ApFe-PLNPs + light. These photo-activated groups were treated with a total of two white light irradiation, at 7-day intervals, at an exposure time of 10 min per mouse. During the entire therapeutic period, there was no significant change in the body weight of all mice (Figure 4b). Similarly, no obvious abnormalities were appeared in the hematoxylin and eosin (H&E) staining of major organs after different treatments (Figure S57). These indicated the negligible toxicity induced by the injection of PLNPs, ApFe-PLNPs and siRNA-ApFe-PLNPs, respectively. The tumor suppression evaluations confirmed that the assistance of photoenergy storage and conversion presented a significant enhancement for antitumor efficiency of these materials (Figures 4c and S58). More specifically, compared with the PBS group, these groups without photo-activation exhibited a limited therapeutic effect, while the photo-activated groups performed a significant inhibition effect of tumor growth. Among these groups, the photo-activated siRNA-ApFe-PLNPs treated group exhibited the best tumor suppression effect, and the tumor volume of these mice was completely suppressed. This can be explained by the fact that combining the excellent photoenergy conversion performance with prominent MTH1 inhibition ability, siRNA-ApFe-PLNPs could lead to a superior antitumor efficacy after photo-excitation. The mice in all groups were dissected and the tumors were collected to take pictures after the therapeutic processes. The weight of tumor tissues (Figure 4d) and tumor images (Figure 4e) also proved the maximized therapeutic effect of siRNA-ApFe-PLNPs after photo-excitation. Moreover, Ki67 and terminal deoxynucleotidyl transferase-mediated dUTP nick end labeling (TUNEL) staining were employed to evaluate the apoptosis and the proliferative capacity of tumors after different treatments, respectively. Ki67 is a well-known biomarker for cellular proliferation, and TUNEL is reported as a general method for detecting apoptosis.[28b,29] The weak red signal of stained Ki67 (Figures 4f and S59) and the vivid green fluorescence of TUNEL staining (Figures 4g and S60) were observed in photo-activated siRNA-ApFe-PLNPs treated tumors, validating the significant suppressed proliferation and evident severer apoptosis. These cumulative pieces of evidence supported that possessing the capacity to store and convert photoenergy, photo-activated siRNA-ApFe-PLNPs enabled the streaming amplification of oxidative stress, causing apoptotic cell death and eventually achieving a prominent antitumor efficacy. The rapid growth and proliferation of tumors can lead to hypoxia tumor microenvironment.[30] The amplification of oxidative stress can efficiently suppress tumor growth, slow down the proliferation of tumor cells, and inhibit the hypoxia of tumor tissues.[4b,28a,e] Additionally, the continuous amplification of oxidative stress could incessantly supply the intratumoral oxygen from nearby tissues, thus alleviating the hypoxia of tumor area.[28e,31] Immunohistochemical staining of HIF-α and VEGF was performed to investigate hypoxia suppression induced by oxidative stress. Reportedly, HIF-α represents a downstream marker of hypoxia and VEGF is a downstream target of HIF-α.[32] The downregulation of HIF-α and VEGF generally indicates the alleviation of tumor hypoxia.[33] It is noticeable that compared with other groups, the photoenergy stored siRNA-ApFe-PLNPs treated group displayed extremely weak brown staining of HIF-α (Figures 4h and S61) and a negligible brown signal of VEGF (Figures 4i and S62), confirming the low expression of HIF-α and VEGF. The downregulation of HIF-α and VEGF in tumor tissues revealed the siRNA-ApFe-PLNPs mediated inhibition of tumor hypoxia after photo-activation. All the above observations manifested that siRNA-ApFe-PLNPs could amplify oxidative stress continuously via efficient photoenergy storage and conversion after photo-excitation, achieving comprehensive in vivo tumor suppression.

Conclusion

In this work, siRNA-ApFe-PLNPs were designed to regulate oxidative stress continuously in tumor cells via effective photoenergy storage and conversion. Under light irradiation, siRNA-ApFe-PLNPs could absorb and store photoenergy. After cessation of excitation, siRNA-ApFe-PLNPs could constantly undergo a Fenton-like reaction by photoenergy conversion, promoting the continuous amplification of oxidative stress. Additionally, siRNA-ApFe-PLNPs were found to hinder MTH1-mediated antioxidant mechanisms, further aggravating oxidative stress and causing apoptotic cell death. In vivo results indicated that HIF-α and VEGF decreased by siRNA-ApFe-PLNPs induced continuous oxidative stress amplification, exhibiting an excellent tumor inhibition effect. Together, photoenergy stored siRNA-ApFe-PLNPs could achieve continuously photo-driven regulation of oxidative stress in the dark, avoiding the photo-induced tissue damage and representing a promising antitumor strategy. These findings provide insights into oxidative stress regulation and reveal a new direction for tumor microenvironment modulation and metabolic pathway regulation.

Acknowledgements

This work was supported by the National Key R&D Program of China (2017YFA0208000), National Natural Science Foundation of China (21925401, 21904037, 22174038, 81874131), Natural Science Foundation of Hunan Province (No. 2020JJ4173).

Conflict of Interest

The authors declare no conflict of interest.

Data Availability Statement

The data that support the findings of this study are available in the supplementary material of this article.

Keywords: Aptamers · Energy-Storage Nanoagent · Nucleic Acids · Oxidative Stress · Photo-Regulation

[1] a) C. Gorrini, I. S. Harris, T. W. Mak, *Nat. Rev. Drug Discovery* **2013**, *12*, 931–947; b) J. Green, M. S. Paget, *Nat. Rev. Microbiol.* **2004**, *2*, 954–966; c) E. Panieri, M. M. Santoro, *Cell Death Dis.* **2016**, *7*, e2253; d) Z. Zhou, J. Song, L. Nie, X. Chen, *Chem. Soc. Rev.* **2016**, *45*, 6597–6626.

[2] a) Q. Chen, J. Zhou, Z. Chen, Q. Luo, J. Xu, G. Song, *ACS Appl. Mater. Interfaces* **2019**, *11*, 30551–30565; b) L. Lin, S. Wang, H. Deng, W. Yang, L. Rao, R. Tian, Y. Liu, G. Yu, Z. Zhou, J. Song, H. H. Yang, Z. Y. Chen, X. Chen, *J. Am. Chem. Soc.* **2020**, *142*, 15320–15330; c) H. Min, Y. Qi, Y. Zhang, X. Han, K. Cheng, Y. Liu, H. Liu, J. Hu, G. Nie, Y. Li, *Adv. Mater.* **2020**, *32*, 2000038.

[3] a) Q. Cheng, W. Yu, J. Ye, M. Liu, W. Liu, C. Zhang, C. Zhang, J. Feng, X. Z. Zhang, *Biomaterials* **2019**, *224*, 119500; b) D. Dominissini, C. He, *Nature* **2014**, *508*, 191–192; c) D. Trachootham, J. Alexandre, P. Huang, *Nat. Rev. Drug Discovery* **2009**, *8*, 579–591; d) J. Wang, Q. Lu, J. Cai, Y. Wang, X. Lai, Y. Qiu, Y. Huang, Q. Ke, Y. Zhang, Y. Guan, H. Wu, Y. Wang, X. Liu, Y. Shi, K. Zhang, M. Wang, A. Peng Xiang, *Nat. Commun.* **2019**, *10*, 5043.

[4] a) C. Liu, Y. Cao, Y. Cheng, D. Wang, T. Xu, L. Su, X. Zhang, H. Dong, *Nat. Commun.* **2020**, *11*, 1735; b) J. Noh, B. Kwon, E. Han, M. Park, W. Yang, W. Cho, W. Yoo, G. Khang, D. Lee, *Nat. Commun.* **2015**, *6*, 6907.

[5] a) O. Babii, S. Afonin, L. V. Garmanchuk, V. V. Nikulina, T. V. Nikolaienko, O. V. Storozhuk, D. V. Shelest, O. I. Dasyukevich, L. I. Ostapchenko, V. Iurchenko, S. Zozulya, A. S. Ulrich, I. V. Komarov, *Angew. Chem. Int. Ed.* **2016**, *55*, 5493–5496; *Angew. Chem.* **2016**, *128*, 5583–5586; b) J. Li, H. Duan, K. Pu, *Adv. Mater.* **2019**, *31*, 1901607; c) Y. Wan, G. Lu, W.-C. Wei, Y.-H. Huang, S. Li, J.-X. Chen, X. Cui, Y.-F. Xiao, X. Li, Y. Liu, X.-M. Meng, P. Wang, H.-Y. Xie, J. Zhang, K.-T. Wong, C.-S. Lee, *ACS Nano* **2020**, *14*, 9917–9928; d) C. Xu, K. Pu, *Chem. Soc. Rev.* **2021**, *50*, 1111–1137; e) S. He, Y. Jiang, J. Li, K. Pu, *Angew. Chem. Int. Ed.* **2020**, *59*, 10633–10638; *Angew. Chem.* **2020**, *132*, 10720–10725; f) Y. Zhang, C. Xu, X. Yang, K. Pu, *Adv. Mater.* **2020**, *32*, 2002661.

[6] Z. Huang, *Technol. Cancer Res. Treat.* **2005**, *4*, 283–293.

[7] Q. Q. Zhan, J. Qian, H. J. Liang, G. Somesfalean, D. Wang, S. L. He, Z. G. Zhang, S. Andersson-Engels, *ACS Nano* **2011**, *5*, 3744–3757.

[8] a) R. Abdurahman, C.-X. Yang, X.-P. Yan, *Chem. Commun.* **2016**, *52*, 13303–13306; b) W. Fan, N. Lu, C. Xu, Y. Liu, J. Lin, S. Wang, Z. Shen, Z. Yang, J. Qu, T. Wang, S. Chen, P. Huang, X. Chen, *ACS Nano* **2017**, *11*, 5864–5872; c) G. Yang, D. Yang, P. Yang, R. Lv, C. Li, C. Zhong, F. He, S. Gai, J. Lin, *Chem. Mater.* **2015**, *27*, 7957–7968.

[9] a) G. Cui, X. Yang, Y. Zhang, Y. Fan, P. Chen, H. Cui, Y. Liu, X. Shi, Q. Shang, B. Tang, *Angew. Chem. Int. Ed.* **2019**, *58*, 1340–1344; *Angew. Chem.* **2019**, *131*, 1354–1358; b) G. Liu, S. Zhang, Y. Shi, X. Huang, Y. Tang, P. Chen, W. Si, W. Huang, X. Dong, *Adv. Funct. Mater.* **2018**, *28*, 1804317; c) J. Wang, Q. Ma, W. Zheng, H. Liu, C. Yin, F. Wang, X. Chen, Q. Yuan, W. Tan, *ACS Nano* **2017**, *11*, 8185–8191; d) Q. Luo, W. Wang, J. Tan, Q. Yuan, *Chin. J. Chem.* **2021**, *39*, 1009–1021.

[10] a) T. Maldiney, A. Bessiere, J. Seguin, E. Teston, S. K. Sharma, B. Viana, A. J. Bos, P. Dorenbos, M. Bessodes, D. Gourier, D. Scherman, C. Richard, *Nat. Mater.* **2014**, *13*, 418–426; b) Z. Pan, Y. Y. Lu, F. Liu, *Nat. Mater.* **2012**, *11*, 58–63; c) L. Song, P.-P. Li, W. Yang, X.-H. Lin, H. Liang, X.-F. Chen, G. Liu, J. Li, H.-H. Yang, *Adv. Funct. Mater.* **2018**, *28*, 1707496.

[11] a) H. Fan, L. Zhang, X. Hu, Z. Zhao, H. Bai, X. Fu, G. Yan, L. H. Liang, X. B. Zhang, W. Tan, *Chem. Commun.* **2018**, *54*, 4310–4313; b) R. W. Williams, G. M. Rubin, *Proc. Natl. Acad. Sci. USA* **2002**, *99*, 6889–6894; c) R. D. Wood, M. Mitchell, T. Lindahl, *Mutat. Res.* **2005**, *577*, 275–283.

[12] a) A. Tuerdi, A. Abdukayum, *RSC Adv.* **2019**, *9*, 17653–17657; b) W. Zhao, C. Zhang, Y. Shi, R. Wu, B. Zhang, *Dalton Trans.* **2015**, *44*, 75–82.

[13] G. Huang, H. Chen, Y. Dong, X. Luo, H. Yu, Z. Moore, E. A. Bey, D. A. Boothman, J. Gao, *Theranostics* **2013**, *3*, 116–126.

[14] a) H. Gad, T. Koolmeister, A. S. Jemth, S. Eshtad, S. A. Jacques, C. E. Strom, L. M. Svensson, N. Schultz, T. Lundback, B. O. Einarsdottir, A. Saleh, C. Gokturk, P. Baranczewski, R. Svensson, R. P. Berntsson, R. Gustafsson, K. Stromberg, K. Sanjiv, M. C. Jacques-Cordonnier, M. Desroses, A. L. Gustavsson, R. Olofsson, F. Johansson, E. J. Homan, O. Loseva, L. Brautigam, L. Johansson, A. Hoglund, A. Hagenkort, T. Pham, M. Altun, F. Z. Gaugaz, S. Vikingsson, B. Evers, M. Henriksson, K. S. Vallin, O. A. Wallner, L. G. Hammarstrom, E. Wiita, I. Almlof, C. Kalderen, H. Axelsson, T. Djureinovic, J. C. Puigvert, M. Haggblad, F. Jeppsson, U. Martens, C. Lundin, B. Lundgren, I. Granelli, A. J. Jensen, P. Artursson, J. A. Nilsson, P. Stenmark, M. Scobie, U. W. Berglund, T. Helleday, *Nature* **2014**, *508*, 215–221; b) K. V. Huber, E. Salah, B. Radic, M. Gridling, J. M. Elkins, A. Stukalov, A. S. Jemth, C. Gokturk, K. Sanjiv, K. Stromberg, T. Pham, U. W. Berglund, J. Colinge, K. L. Bennett, J. I. Loizou, T. Helleday, S. Knapp, G. Superti-Furga, *Nature* **2014**, *508*, 222–227.

[15] J. Wang, Q. Ma, X. X. Hu, H. Liu, W. Zheng, X. Chen, Q. Yuan, W. Tan, *ACS Nano* **2017**, *11*, 8010–8017.

[16] L. Peng, M. X. You, C. C. Wu, D. Han, I. Ocsoy, T. Chen, Z. Chen, W. H. Tan, *ACS Nano* **2014**, *8*, 2555–2561.

[17] J. Hu, Z. Zhao, Q. Liu, M. Ye, B. Hu, J. Wang, W. Tan, *Chem. Asian J.* **2015**, *10*, 1519–1525.

[18] a) A. Babu, R. Muralidharan, N. Amreddy, M. Mehta, A. Munshi, R. Ramesh, *IEEE Trans. Nanobiosci.* **2016**, *15*, 849–863; b) D. Semizarov, P. Kroeger, S. Fesik, *Nucleic Acids Res.* **2004**, *32*, 3836–3845.

[19] a) M. Huo, L. Wang, Y. Chen, J. Shi, *Nat. Commun.* **2017**, *8*, 357; b) F. Yu, Y. Huang, A. J. Cole, V. C. Yang, *Biomaterials* **2009**, *30*, 4716–4722.

[20] a) Y. Du, C. Yang, F. Li, H. Liao, Z. Chen, P. Lin, N. Wang, Y. Zhou, J. Y. Lee, Q. Ding, D. Ling, *Small* **2020**, *16*, 2002537; b) Y. Fu, X. Zhao, J. Zhang, W. Li, *J. Phys. Chem. C* **2014**, *118*, 18116–18125.

[21] a) P. Bilski, K. Reszka, M. Bilska, C. F. Chignell, *J. Am. Chem. Soc.* **1996**, *118*, 1330–1338; b) Z. Zhai, S. E. Gomez-Mejiba, D. C. Ramirez, *Inflammation* **2013**, *36*, 346–354.
[22] a) S. G. Crich, E. Terreno, S. Aime, *Adv. Drug Delivery Rev.* **2017**, *119*, 61–72; b) Y. Hu, S. Mignani, J. P. Majoral, M. Shen, X. Shi, *Chem. Soc. Rev.* **2018**, *47*, 1874–1900.
[23] a) B. Ding, S. Shao, H. Xiao, C. Sun, X. Cai, F. Jiang, X. Zhao, P. Ma, J. Lin, *Nanoscale* **2019**, *11*, 14654–14667; b) M. Duan, F. Xia, T. Li, J. G. Shapter, S. Yang, Y. Li, G. Gao, D. Cui, *Nanoscale* **2019**, *11*, 18426–18435; c) D. Wang, D. B. Cheng, L. Ji, L. J. Niu, X. H. Zhang, Y. Cong, R. H. Cao, L. Zhou, F. Bai, Z. Y. Qiao, H. Wang, *Biomaterials* **2021**, *264*, 120386; d) L. Zeng, L. Xiang, W. Ren, J. Zheng, T. Li, B. Chen, J. Zhang, C. Mao, A. Li, A. Wu, *RSC Adv.* **2013**, *3*, 13915–13925.
[24] L. Zhang, S. S. Wan, C. X. Li, L. Xu, H. Cheng, X. Z. Zhang, *Nano Lett.* **2018**, *18*, 7609–7618.
[25] H. Ranji-Burachaloo, P. A. Gurr, D. E. Dunstan, G. G. Qiao, *ACS Nano* **2018**, *12*, 11819–11837.
[26] a) O. Myhre, J. M. Andersen, H. Aarnes, F. Fonnum, *Biochem. Pharmacol.* **2003**, *65*, 1575–1582; b) J. Zhang, X. Qin, B. Wang, G. Xu, Z. Qin, J. Wang, L. Wu, X. Ju, D. D. Bose, F. Qiu, H. Zhou, Z. Zou, *Cell Death Dis.* **2017**, *8*, e2954.
[27] a) Z. Ding, P. Liu, D. Hu, Z. Sheng, H. Yi, G. Gao, Y. Wu, P. Zhang, S. Ling, L. Cai, *Biomater. Sci.* **2017**, *5*, 762–771; b) Y. Sun, Z. L. Chen, X. X. Yang, P. Huang, X. P. Zhou, X. X. Du, *Nanotechnology* **2009**, *20*, 135102; c) L. Yan, A. Amirshaghaghi, D. Huang, J. Miller, J. M. Stein, T. M. Busch, Z. Cheng, A. Tsourkas, *Adv. Funct. Mater.* **2018**, *28*, 1707030.
[28] a) N. Gong, X. Ma, X. Ye, Q. Zhou, X. Chen, X. Tan, S. Yao, S. Huo, T. Zhang, S. Chen, X. Teng, X. Hu, J. Yu, Y. Gan, H. Jiang, J. Li, X. J. Liang, *Nat. Nanotechnol.* **2019**, *14*, 379–387; b) L. Kou, R. Sun, X. Jiang, X. Lin, H. Huang, S. Bao, Y. Zhang, C. Li, R. Chen, Q. Yao, *ACS Appl. Mater. Interfaces* **2020**, *12*, 30031–30043; c) H. Lin, Y. Chen, J. Shi, *Chem. Soc. Rev.* **2018**, *47*, 1938–1958; d) S. Park, B. Kwon, W. Yang, E. Han, W. Yoo, B. M. Kwon, D. Lee, *J. Controlled Release* **2014**, *196*, 19–27; e) J. Zou, J. Zhu, Z. Yang, L. Li, W. Fan, L. He, W. Tang, L. Deng, J. Mu, Y. Ma, Y. Cheng, W. Huang, X. Dong, X. Chen, *Angew. Chem. Int. Ed.* **2020**, *59*, 8833–8838; *Angew. Chem.* **2020**, *132*, 8918–8923.
[29] I. Kalashnikova, J. Mazar, C. J. Neal, A. L. Rosado, S. Das, T. J. Westmoreland, S. Seal, *Nanoscale* **2017**, *9*, 10375–10387.
[30] S. S. Sabharwal, P. T. Schumacker, *Nat. Rev. Cancer* **2014**, *14*, 709–721.
[31] H. Chen, A. Ma, T. Yin, Z. Chen, R. Liang, H. Pan, X. Shen, M. Zheng, L. Cai, *ACS Appl. Mater. Interfaces* **2020**, *12*, 12573–12583.
[32] a) A. L. Harris, *Nat. Rev. Cancer* **2002**, *2*, 38–47; b) A. Kaidi, A. C. Williams, C. Paraskeva, *Nat. Cell Biol.* **2007**, *9*, 210–217; c) J. Pouysségur, F. Dayan, N. M. Mazure, *Nature* **2006**, *441*, 437–443.
[33] Y. Hu, X. Wang, P. Zhao, H. Wang, W. Gu, L. Ye, *Biomater. Sci.* **2020**, *8*, 2931–2938.

Manuscript received: January 6, 2022
Accepted manuscript online: January 22, 2022
Version of record online: ■■, ■■

Research Articles

Antitumor Agents

C. Ji, H. Li, L. Zhang, P. Wang, Y. Lv, Z. Sun,* J. Tan,* Q. Yuan,* W. Tan e202200237

Ferrocene-Containing Nucleic Acid-Based Energy-Storage Nanoagent for Continuously Photo-Induced Oxidative Stress Amplification

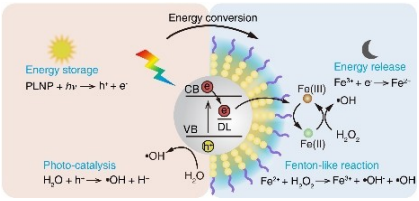

The siRNA-aptamer-ferrocene modified persistent luminescence nanoparticle (siRNA-ApFe-PLNP) was designed as an energy-storage nanoagent to achieve continuous amplification of oxidative stress after photo-activation, eliminating the need for constant light irradiation and further avoiding the photo-induced tissue damage.